Magnetic Phase Diagram of $Cr_{100-x}Os_x$ alloys

PR Fernando[1], ARE Prinsloo[1], CJ Sheppard[1] and JAL Lodya[2]

[1]Department of Physics, University of Johannesburg, PO Box 524, Auckland Park, 2006, South Africa
[2]Sasol Technology, Research & Development, 1, Klasie Havenga Road, Sasolburg, 1947, South Africa

Author e-mail address: alettap@uj.ac.za

Abstract: The magnetic phase diagram of $Cr_{100-x}Os_x$ exhibits a triple point at T_L = 315 K and x_L = 0.14, where the incommensurate (I) spin-density-wave (SDW), commensurate (C) SDW and paramagnetic (P) phases coexist. Previous studies focused on measurements around the triple point and concentrations up to x = 2. The possible merits of an investigation into the magnetic phase diagram of Cr-Os specifically at high diluent concentrations should be considered against the background of other Cr alloys with group-8 diluents, such as those of Cr-Re and Cr-Ru. These alloys show interesting features for $x >> x_L$, such as superconducting properties and quantum critical behaviour. Thus, in order to initiate similar studies a polycrystalline $Cr_{100-x}Os_x$ alloy series with $2 < x < 22$ were prepared and characterized using scanning electron microscopy, electron microprobe analysis and X-ray diffraction. Electrical resistivity (ρ) and magnetization (M) measurements as a function of temperature (T) were done in the temperature range of 2 K < T < 1100 K. These results were used to obtain the Néel transition temperatures (T_N) of the various alloys and to map out the magnetic phase diagram of the $Cr_{100-x}Os_x$ alloy system for $x > 2$.

1. Introduction

The magnetic phase diagram of $Cr_{100-x}Os_x$ exhibits a triple point at T_L = 315 K and x_L = 0.14, where the incommensurate (I) spin-density-wave (SDW), commensurate (C) SDW and paramagnetic (P) phases coexist [1, 2]. Previous studies on the physical properties of Cr-Os included heat capacity (C_p) [2], electrical resistivity (ρ) [2, 3, 4], thermal expansion [2, 4] and magnetic susceptibility (χ) [5, 6]. These studies focused on measurements around the triple point and concentrations up to x = 2, leaving the phase diagram of Cr-Os incomplete for $x \gg x_L$.

It is surprizing that the Cr-Os magnetic phase diagram has not been fully explored and is still unknown for concentrations above x = 2 [1-6], as the magnetic phase diagrams of many Cr alloys with group-8 metals, such as Cr with Re and Ru have very interesting properties for $x \gg x_L$ [1]. These properties include possible superconducting behaviour existing together with antiferromagnetism [1], as well as quantum critical behaviour [7, 8]. These properties are strongly associated with current interests as is revealed in recent literature [7-12]. Superconducting properties in Cr-Os alloys with very high concentrations of Os have been previously reported [13, 14, 15]. Alloys containing 25, 28 and 33 at.% Os show superconducting transition temperature (T_s) at 2.4 and 2.75, 4.03 and 1.03 K, respectively [13, 14, 15]. This is in agreement with results obtained for other alloys with group-8 diluents such as in the case of Cr-Ir, Cr-Ru and Cr-Rh [14, 16].

In order to extend the investigations of the unique properties of Cr alloys with group-8 diluents and to be ultimately inclusive of all Cr alloys with group-8 metals, the present investigation focusses on

the properties of the $Cr_{100-x}Os_x$ alloys with $2 \leq x \leq 22$. This study utilizes electrical resistivity (ρ) and magnetization (M) measurements in order to complete the phase diagram of $Cr_{100-x}Os_x$, from which further investigations can follow.

2. Experimental

Polycrystalline binary $Cr_{100-x}Os_x$ alloys with $2 \leq x \leq 22$ were prepared by arc melting in a purified low pressure argon atmosphere from Cr and Os of mass fractional purities 99.999% and 99.99% respectively. The constituent metals were melted fifteen times in total, turning it upside down between melts with two crushes after every five melts in order to improve the homogeneity. Powder X-ray diffraction (XRD) analyses, using Cu-K_α was used to characterize the samples structurally and confirm whether the samples were single or multi-phase. The actual elemental composition and homogeneity were determined using electron microprobe analyses. Electrical resistivities (ρ) were measured in the range $2 \leq T \leq 380$ K, using the Quantum Design Physical Properties Measurement System (PPMS) incorporating the appropriate measurement option. Resistivity measurements for the temperature range 273 K to 1100 K were performed under high vacuum using the standard dc-four probe method with Keithley instrumentation. In order to eliminate the thermal EMF the sample current was reversed for each set of readings [17]. For samples with transitions in a range $300 \text{ K} \leq T \leq 700$ K the PPMS with the vibrating sample magnetometer (VSM) oven option were used to measure the magnetization (M) on heating in an applied magnetic field of 20 kOe. The Quantum Design Magnetic Property Measurement System (MPMS) was used to measure the magnetization for samples with transitions in the temperature range $2 \text{ K} \leq T \leq 390$ K. These samples were zero field cooled (ZFC) to 2 K and measurements were taken on heating in an applied magnetic field of 50 Oe.

3. Results and discussion

Figure 1(a) and (b) show the X-ray diffraction (XRD) spectra of the as-cast $Cr_{98}Os_2$ and $Cr_{87}Os_{13}$ in grey, while the XRD spectrum for pure Cr is shown in black. The XRD spectra were compared to that in the Joint Council of Powder Diffraction Database (JCPDD) for pure body centred cubic (bcc) Cr (reference number: 04-008-5987). Comparing the relative peak positions, obtained from the JCPDD data base to the current XRD spectra of $Cr_{98}Os_2$ and $Cr_{87}Os_{13}$, it is observed that only the primary reflections [110], [200], [211] and [220] were obtained. The absence of any other reflections, which might be observed for other Cr-Os binary alloys, indicates that the current alloys were in single phase. Since annealing of the samples created additional phases it was decided to only use as-cast samples in the present study.

It is also observed in figure 1(a) and (b) that for the Cr-Os alloys the primary reflections are slightly shifted to lower 2θ values, relative to the primary peak positions of pure Cr. This displacement is more apparent for $Cr_{87}Os_{13}$ than for $Cr_{98}Os_2$ though, i.e. it increases with increasing

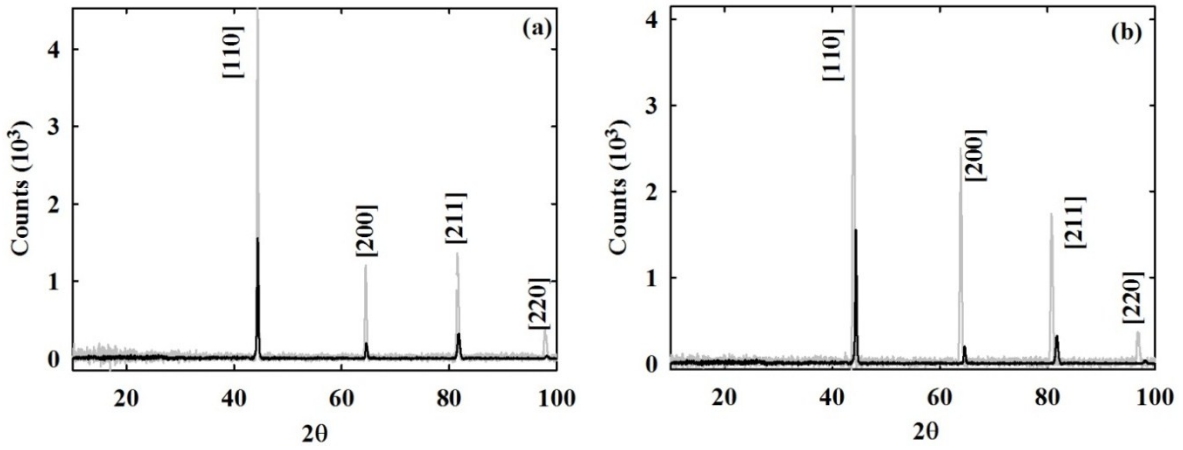

Figure 1. XRD patterns for (a) $Cr_{98}Os_2$ and (b) $Cr_{87}Os_{13}$ alloys are shown in grey, together with the pattern expected for pure Cr shown in black. The (*hkl*) Miller indices of the various reflections obtained from the JCPDD expected for the profile of bcc Cr are indicated (reference number: 04-008-5187).

Os concentration. It is believed that the shift is caused by a distortion in the lattice parameter due to the addition of the large Os atoms. The lattice parameters (a) as function of x for $Cr_{100-x}Os_x$ alloys, as calculated from the XRD results, are represented by solid circles figure 2. The lattice parameter increased linearly from the value of 0.28800 nm obtained for pure Cr to 0.29108 nm for the $Cr_{78}Os_{22}$ alloy. Following the work of Vagard [18] the theoretically expected lattice parameters were calculated using:

$$a_{\text{alloy}} = (1 - x)a_{\text{Cr}} + xa_{\text{Os}}, \quad (1)$$

where a_{Cr} and a_{Os} refer to the lattice parameters of Cr and Os at room temperature, respectively, and a_{alloy} is the calculated value for the lattice parameter for the specific $Cr_{100-x}Os_x$ alloy. The values obtained using equation (1) is represented by the open triangles in figure 2, these correspond well with those calculated from XRD results. A linear fit, $a = bx + c$, to the data in the investigated concentration range gives $b = (1.411\times10^{-3} \pm 2.546\times10^{-5})$ Å/at.% Os and $c = (2.88 \pm 3.241\times10^{-4})$ Å.

Electron microprobe analyses of the Cr-Os alloys indicate that all the samples are homogeneous in composition and that the actual concentrations of the Os vary by less than 1 at.% from the nominal concentrations. The relatively small deviation in the actual and nominal concentrations can be attributed to mass losses during the manufacturing process of Cr alloys, due to the evaporation and diffusion of tiny mass particles during melting and/or to the mass losses during crushing process.

Representative $\rho(T)$ curves for $Cr_{100-x}Os_x$ alloys with $2 \le x \le 22$ are shown in figures 3(a) and (b). Well defined anomalies appear in the form of clear minima followed by prominent domes in all the $\rho(T)$ curves for alloys with $x \le 13$. This behaviour is associated with the formation of the SDW on entering the antiferromagnetic phase on cooling through the Néel temperature (T_N) [1]. The sudden increase in resistivity on cooling through T_N finds its origin in the nesting of electron and hole Fermi surfaces [1]. This leads to a reduction in the charge carriers available for conduction resulting in an increase in resistivity just below T_N [1]. The anomalies become more pronounced on increasing the Os concentration up to $x = 4$, as the electron and hole Fermi surfaces become increasingly similar in size. Greater parts of the Fermi surfaces are thus being affected, causing an increase in the resistivity anomalies as the SDW becomes more commensurate [3, 19] with the lattice. However, for alloys with $x \ge 6$ it is observed that the relative size of the magnetic anomalies, as well as the values of T_N, decreases.

The Néel temperature for Cr alloys can be defined either as the temperature of the minimum in $\rho(T)$ accompanying the magnetic phase transition or the inflection point in $\rho(T)$ curve; determined by considering the temperature associated with the minimum in $d\rho/dT$ versus T curve[1]. Considering all the results obtained it was decided to implement the first definition of T_N for the present study regarding the magnetic phase transitions in the $Cr_{100-x}Os_x$ alloy system.

Figure 4 shows representative reduced magnetization, $M_r(T)$, curves for $Cr_{100-x}Os_x$ alloys. For measurements the temperature range 300 K < T < 700 K M_r is defined as M/M_{300K}, while for measurements the range 2 K < T < 300 K, $M_r = M/M_{2K}$. The dashed lines in figure 4(a) and the inset of figure 4(b) represents a back extrapolation from the paramagnetic phase at $T > T_N$. The T_N values

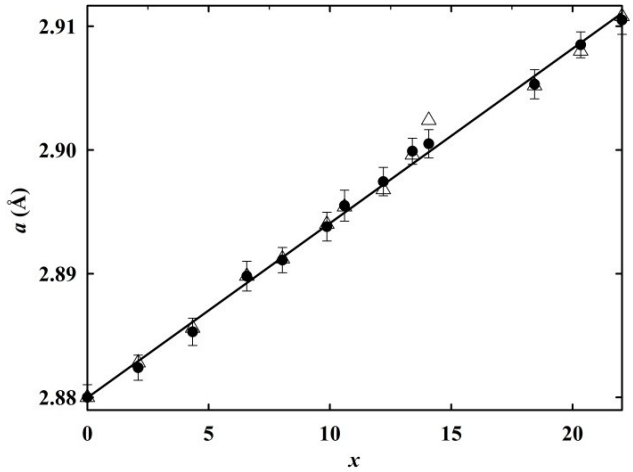

Figure 2. The lattice constant (a) as function of x for various $Cr_{100-x}Os_x$ alloys. The values obtained from the XRD measurements are represented by the solid circles (•) with error bars. Open triangles (△) represent the values obtained using $a_{\text{alloy}} = (1 - x)a_{\text{Cr}} + xa_{\text{Os}}$, where a_{Cr} and a_{Os} refer to the lattice parameters of Cr and Os at room temperature, respectively, and a_{alloy} is the calculated value of the lattice parameter for each specific $Cr_{100-x}Os_x$ alloy [18]. The line is a linear fit to the experimental data.

indicated by arrows were obtained from the point where the $M_r(T)$ curve deviates from the dashed line. Anomalies, in the form of a downturn on cooling, are observed in the vicinity of T_N for the alloys with $x < 13$, similar to the behaviour normally observed for Cr alloys below T_N [1]. The downturn in $M_r(T)$ on cooling through T_N is ascribed to a decrease in the density of states at the Fermi surface when the nested parts of the electron and hole Fermi sheets are annihilated. The decrease in the density of states is accompanied by a decrease in the itinerant electron concentration responsible for magnetism [1]. It is again noted that the anomalies become more pronounced for Cr-Os alloys approaching the concentration $x = 4$, after which a further increase in Os content results in an increasingly weaker anomaly in the $M_r(T)$ curves at T_N. As an example of this, consider the $M_r(T)$ curve of the $x = 12$ alloy shown in figure 4(b). A relatively weak anomaly at T_N for this alloy (at approximately 150 K) is hardly visible in the full scale curve, it is however clearly seen on an enlarged scale on the inset shown in figure 4(b). The results of the $x = 12$ alloy show a slight increase in M_r when cooling from $T > T_N$, followed by the expected downturn for $T < T_N$, resulting in a weak

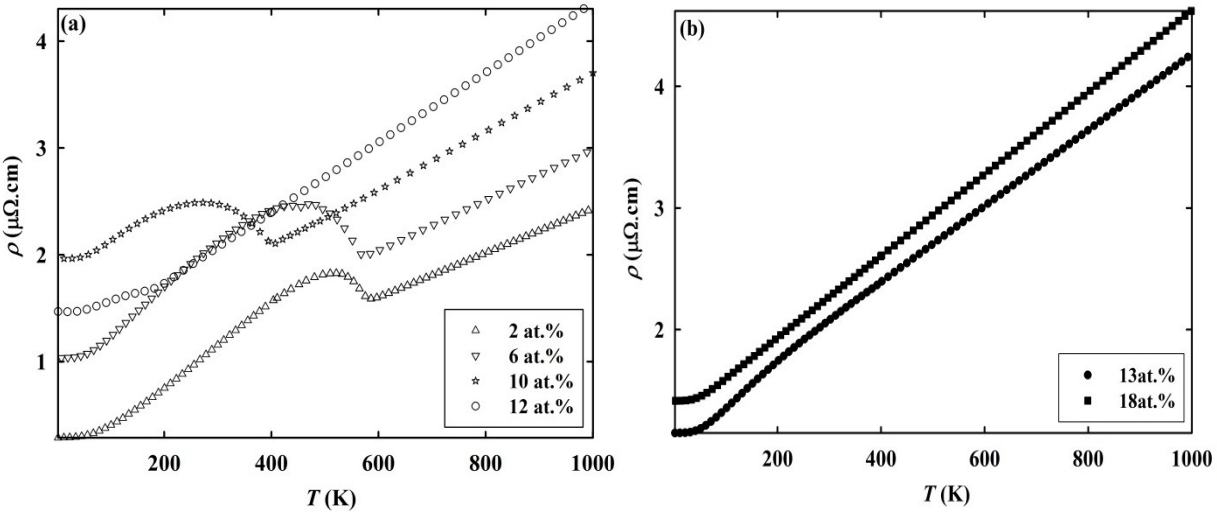

Figure 3 (a) and (b). The electrical resistivity, ρ, of selected $Cr_{100-x}Os_x$ alloys in the temperature range $2 \leq T \leq 1000$ K, with (a) $x = 2$ (△), 6 (▽), 10 (☆) and 12 (○) and, (b) $x = 13$ (•) and 18 (■).The experimental error in the absolute value of ρ is approximately 3% and originates mainly from errors in the determination of the sample dimensions.

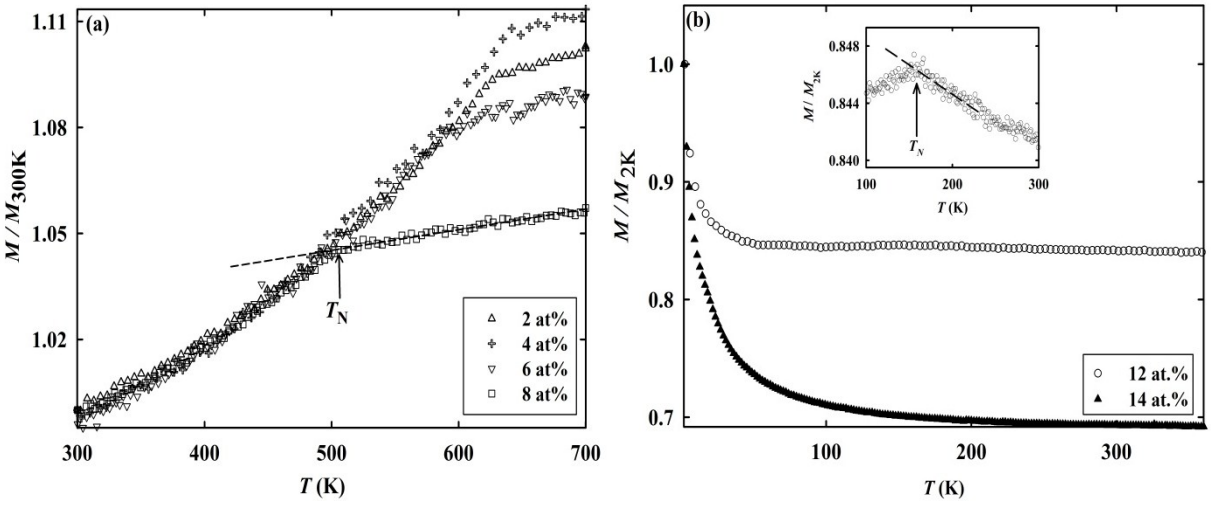

Figure 4. The temperature dependence of the magnetization, $M_r(T)$, of the $Cr_{100-x}Os_x$ alloy system with (a) $x = 2$ (△), 4 (+), 6 (▽) and 8 (□) in the temperature range 300 to 700 K and, (b) $x = 12$ (○) and 14 (▲) in the temperature range 2 to 390 K. The inset in (b) shows $M_r(T)$ curve for $x = 12$ on an enlarged scale. The dashed lines are discussed in the text.

peak in $M_r(T)$ at T_N. Alloys with $x > 13$ did not show anomalous behaviour associated with a magnetic transition in their $M_r(T)$ curves in the temperature range 2 to 390 K – see for example the $M_r(T)$ curve for the $x = 14$ alloy shown in figure 4(b). These samples were taken to be paramagnetic at all temperatures down to 2 K.

In figure 5 the magnetic phase diagram for the Cr-Os alloys is shown, constructed from the T_N values obtained from the current $\rho(T)$ and $M(T)$ results, together with those determined in previous studies [2-6]. It is evident that the T_N values obtained from the current $\rho(T)$ results correspond well with those found in previous studies on this alloy system for $x = 2$. However, discrepancies are observed in the T_N values obtained from the $\rho(T)$ and $M(T)$ results for samples with $x = 2$, 4, 6, 8, 10 and 12. Resistivity measurements are known to be extremely sensitive to anomalies at T_N and are normally the first type of measurements to be considered in determining the magnetic transition temperatures [1]. As mentioned earlier, the $M(T)$ results for these samples were obtained using the VSM option of PPMS that could be used for measurements in the temperature range 300 to 700 K, while $M(T)$ results for the samples with $x > 8$ was obtained from magnetization measurements utilizing the MPMS in a temperature range 2 to 400 K. From figure 5 it is clear that the T_N values obtained from the $M(T)$ results using the VSM option of the PPMS differ to a larger extend from those determined from the $\rho(T)$ results, when compared to those T_N values obtained from the $M(T)$ results obtained using the MPMS. It is speculated that these discrepancies can possibly be related to the differences in heating rates (0.6 K/min for the MPMS versus 5 K/min for the PPMS) or the differences in the applied magnetic fields (50 Oe for the MPMS versus 20 kOe for the PPMS, i.e. relatively high applied magnetic fields were required to effect magnetic transitions with the VSM oven option). On the other hand it is also important to remember that the MPMS is equipped with a more sensitive SQUID sensor, thus enabling extremely accurate magnetic measurements, two orders of magnitude better than the magnetization values obtained using a VSM option of the PPMS [19, 20]. However, the reasons for the observed discrepancies still warrant further investigation.

The present study extends the magnetic phase diagram of this alloy system to much higher Os diluent concentrations than what were previously determined [2-6]. The magnetic phase diagram obtained for $Cr_{100-x}Os_x$ alloy system resembles the typical behaviour of Cr alloys with group-8 metals. The initial increase in T_N with increasing Os concentration can be understood by Fedders and Martin's theory [3, 5, 17, 21-23]. According to this theory, addition of metals to the right of Cr in the periodic table increases the electron to atom ratio (e/a) and the size of the electron Fermi sheet of pure Cr. This leads to an increase in the contact area between the electron and hole sheets which correspond to an increase in T_N [24]. Applied to the current alloy system this implies that the Os increases the electron concentration and enlarges the interaction area of the electron-hole Fermi surfaces. This effect

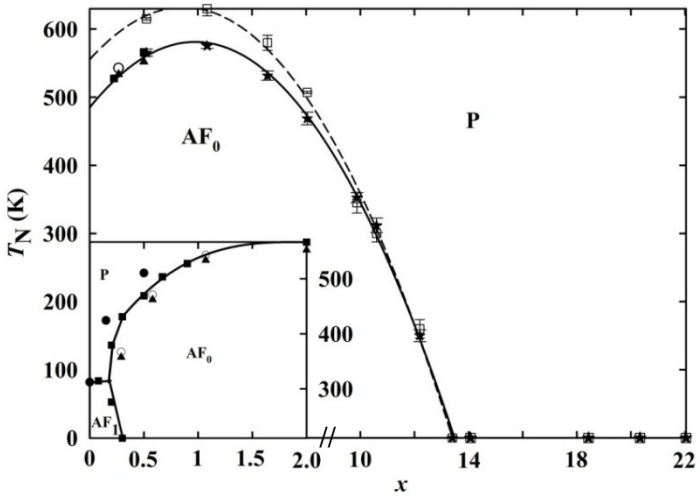

Figure 5. The magnetic phase diagram for the $Cr_{100-x}Os_x$ alloy system as function of Os concentration, showing T_N (K) values obtained from electrical resistivity (★) and magnetization (□) in the present study. Data points from previous studies are also shown in the figure: Arajs *et al.* [3] (●), Butylenko *et al.* [1, 2, 4] (▲,■) and Hedman *et al.* [5] (○). P refers to the paramagnetic phase, while AF_1 and AF_0 refer to the incommensurate and commensurate SDW phases, respectively. The solid and dashed lines are guides to the eye.

improves the nesting and stabilises the SDW. As x is increased, the CSDW phase forms at $x = x_L$. On addition of Os concentration above triple point concentration, T_N rises rapidly and reaches saturation at approximately 4 at.% Os, where perfect nesting occurs, when the size of electron sheet becomes nearly equal to the hole sheet. Further addition of Os leads to Fermi surface mismatch again and the electron sheet becomes bigger than the hole sheet. This effect destabilizes the structure and reduces the T_N. According to the current results, the antiferromagnetic order is completely suppressed for Cr-Os alloys with $x > 13$ and samples with $x > 13$ remain paramagnetic for all $T > 2$ K.

4. Conclusion

The magnetic phase diagram of $Cr_{100-x}Os_x$ alloy system was, for the first time, as could be ascertained, determined for concentrations as high as $x = 22$. The general behaviour is similar to that observed for other Cr alloys with group-8 non-magnetic transition metals such as Cr-Ru and Cr-Re [1]. It is important to note that the present $\rho(T)$ results fit well in with those obtained from previous studies [2-6] on this system for $x < 2$ and shows that the antiferromagnetism in this system appears to be fully suppressed for $x = 13$. However, discrepancies is observed in the T_N values obtained from the $\rho(T)$ and $M(T)$ results for samples with $x = 2$, 4, 6, 8, 10 and 12 – this needs to be clarified through further investigation. No indication of superconductivity was found in the $\rho(T)$ measurements of the alloys investigated, in the temperature range $T > 2$ K.

This project has addressed certain fundamental questions regarding the behaviour of the Cr-Os magnetic phase diagram at relatively high diluent concentrations. This is a first step from where investigations into possible quantum criticalities in this alloy system can follow.

Acknowledgments Financial support from the South African NRF (Grant numbers 80928 and 80626) and the Faculty of Science from the University of Johannesburg is acknowledged.

References

[1] Fawcett E, Alberts HL, Galkin VY, Noakes DR and Yakhmi JV 1994 *Rev. Mod. Phys.* **66** 25
[2] Butylenko AK and Nevadcha VV 1982 *Sov. Phys. Tech. Phys.* **27**(1) 102
[3] Arajs S, De Young F. Tice and Andreson E E 1970 *J. Appl. Phys*. **41**(3) 1426
[4] Butylenko AK 1985 *Sov. Phys. Tech. Phys*. **30** (8) 942
[5] Moyer C A, Kelly J R, Arajs S, Kote G and Garbe K 1981 *J. Appl .Phys*. **52**(3) 1643
[6] Booth J G 1964 *Phys. Stat. Sol.* **7** K157
[7] Jacobs BS, Prinsloo ARE, Sheppard CJ and Strydom AM 2013 *J. Appl. Phys*. **113** 17E126
[8] Reddy L, Alberts HL, Strydom AM, Prinsloo ARE and Venter AM 2008 *J. Appl. Phys.* **103** 07C903
[9] Yeh A, Soh Y-A, J Brooke J, Aeppli G, Rosenbaum TF and Hayden SM 2002 *Nature* **419** 459
[10] Lee M, Husmann A, Rosenbaum TF and Aeppli G 2004 *Phys. Rev. Lett*. **92**(18) 187201
[11] Jaramillo R, Feng Y, Wang J and Rosenbaum TF 2010 Proc. Nat. Acad. of Sci. USA (PNAS) **107**(9) 09E116
[12] Sheppard CJ, Prinsloo ARE, Alberts HL and Strydom AM 2011 *J. Appl. Phys*. **109**(7) 07E104
[13] Venkatraman M and Neumann JP 1990 *Bulletin of Alloy Phase Diagrams*. **11**(1) 8
[14] Blakgher RD, Hein RE, Cox JE and Waterstrat RM 1969 *J. Low. Temp. Phys.* **1** (6) 539
[15] Fluliger R, Paoli A and Muller J 1974 *Solid State Commun.* **14** 443
[16] Matthias BT, Geballe TH, Compton VB, Corenzwit E and Hull GW 1962 *Phys. Rev.* **128**(2) 588
[17] Gopalakrishnan IK,Yakhmi JV and Iyer RM 1984 *J. Magn. Magn. Mat*. **46** 207
[18] Denton AR and Ashcroft NW 1991 *Phys. Rev*. *A*. **43**(6) 3161
[19] PPMS MultiVu Application User's Manual 2008 Rev.A2
[20] MPMS MultiVu Application User's Manual 1999 Rev.A2
[21] De Young TF, Arajs S and Anderson EE 1971 *Amer. Inst. Phys. Conf. Proc. Magn and Magn. Mat*. **5** 517
[22] Fukamichi K and Siato H 1975 *J. Less Common Met.* **40** 357
[23] Fedders PA and Martin PC 1966 *Phys. Rev*. **143**(1) 245
[24] Yakhmi JV, Gopalakrishnan IK and Iyer RM 1983 *J. Less Common Met*. **91** 327